processes

MDPI

Article

Optimizing the Geometric Parameters of a Stepped Labyrinth Seal to Minimize the Discharge Coefficient

Ye Hwan Chun [1] and Joon Ahn [2,*]

[1] Department of Mechanical Engineering, Graduate School, Kookmin University, 77 Jeongneung-ro, Seongbuk-gu, Seoul 02707, Korea
[2] School of Mechanical Engineering, Kookmin University, Seoul 02707, Korea
* Correspondence: jahn@kookmin.ac.kr

Abstract: A series of numerical simulations were performed to study the discharge coefficient based on the geometric parameters of a stepped labyrinth seal that sealed the secondary flow path of a gas turbine. In contrast with straight-through seals, stepped labyrinth seals introduce additional geometrical parameters related to the steps. In this study, three shape variables were observed: step height (SH), position, and cavity width (CW). The sensitivity to the leakage flow of the shape variable in the stepped labyrinth seal was analyzed. The mechanism for improving the sealing performance of stepped labyrinth seals was investigated. The results indicated that the stepped labyrinth seal exhibited up to 17.9% higher leakage-suppression performance than the straight labyrinth seal. Seals with large discharge coefficients had a large vena contracta upstream of each tooth structure and a rapidly accelerated axial velocity in the radial direction. We could observe that the discharge coefficient changed according to the flow field in the cavity. The wall shear stress was sensitive to the SH but not to the CW or step position.

Keywords: discharge coefficient; vena contracta; labyrinth seal; gas turbine; Reynolds-averaged Navier–Stokes (RANS)

Citation: Chun, Y.H.; Ahn, J. Optimizing the Geometric Parameters of a Stepped Labyrinth Seal to Minimize the Discharge Coefficient. *Processes* **2022**, *10*, 2019. https://doi.org/10.3390/pr10102019

Academic Editor: Blaž Likozar

Received: 14 September 2022
Accepted: 22 September 2022
Published: 6 October 2022

1. Introduction

Gas turbines operate according to the Brayton cycle. Several methods have been proposed to increase the efficiency of gas turbines in the Brayton cycle. Among them, the most effective method is the use of a technique that improves efficiency when the turbine inlet temperature increases [1]. However, turbine blades are damaged when the turbine inlet temperature increases. Therefore, the damage is reduced by applying film cooling to the turbine blades [2,3].

The film-cooling method extracts cooling fluid from a compressor and supplies it to the turbine blades through a secondary flow path. The secondary flow path consists of rotating and stationary parts according to the characteristics of the rotating machine. A gap inevitably occurs between the static and rotating parts, and some cooling fluid leaks through this gap.

Zhou investigated the causes of the reduction in the efficiency of gas turbines and reported that leakage that occurred in the gap between the stationary and rotating parts caused the third largest effect out of 13 factors [4]. A seal is needed to suppress these leaks [5]. If a contact seal is used, the leakage flow can be effectively stopped. However, seal damage due to friction or thermal expansion is highly possible. Therefore, labyrinth, brush, and honeycomb seals are used [6–8], and the labyrinth seal is widely used because it can easily be manufactured [9].

A significant portion of the cooling fluid leaks through the secondary flow path. This factor hinders the increase in the turbine inlet temperature. Therefore, a labyrinth seal that can suppress this leak is required. A predictable model or equation is needed to

design the labyrinth seal under each condition. Becker et al. explained the fluid flow in a straight labyrinth seal, modeled the Poiseuile flow, and investigated the friction coefficient [10]. Stodola et al. predicted a straight-labyrinth-seal leakage flow using Bernoulli's principle and continuity equation but did not consider the kinetic energy in the cavity [11]. Martin et al. derived a straight-labyrinth-seal leakage-flow equation for the first time [9]. Egli et al. stated that the flow using a straight labyrinth seal was similar to that of an orifice, assuming that the kinetic energy in the cavity was dissipated and the effect of the number of tooth structures on the leakage flow was considered [12]. Hodkinson et al. analyzed the kinetic energy transmitted to the next cavity by a flow that passed through the gap. They predicted the leakage flow using the kinetic-energy carry-over coefficient [13]. Dollin et al. reported that the leakage flow was small because Martin's equation was assumed to be isothermal [14].

After the first straight labyrinth seal was modeled or an equation was derived, several researchers derived a modified model or equation through experiments. Jeri et al. reported that the tooth-structure height was dimensionless relative to the cavity width (CW) and that the leakage flow increased when this ratio was very high [15]. Wittig et al. obtained various non-dimensionalized shape variables and derived the leakage-flow rate of a straight labyrinth seal as an isotropic entropy equation through experiments [16–18].

The straight labyrinth seal offers no option but requires a design for a significant clearance gap that considers the rotor deviation. In addition, using many tooth structures is difficult because the space into which the labyrinth seal is installed is limited. Therefore, shape-optimization design research for straight labyrinth seals was conducted. Researchers devised a method for optimizing the leakage-flow reduction using a numerical model. Baek et al. optimized the shape of a straight labyrinth seal using a Reynolds-averaged Navier–Stokes (RANS) model [19–21]. Wein et al. analyzed a straight labyrinth seal using various RANS models and reported that the mass flow through the flow field and straight labyrinth seal varied according to the RANS model [22,23].

A new labyrinth seal was developed, as shown in Figure 1, by breaking away from the stereotype of a straight labyrinth seal, which is the primary form of the labyrinth seal. Stoker et al. developed an advanced labyrinth seal that reduced the leakage flow by modifying a straight labyrinth seal [24,25]. Wittig et al. derived a model through experiments and numerical analyses on the leakage-flow rate and heat transfer of a stepped labyrinth seal [26]. Hur et al. selected the clearance gap of the stepped labyrinth seal as a shape variable and optimized the shape using numerical analyses [27–29]. Vakili et al. calculated the discharge coefficient according to the pressure ratio of the stepped labyrinth seal. They studied the viscous loss through experiments and employed a two-dimensional (2D) axisymmetric modeling computational fluid dynamic analysis [30]. However, no discussion was presented on the cause of the change in the discharge coefficient or in determining the optimal design point that considered various shape variables.

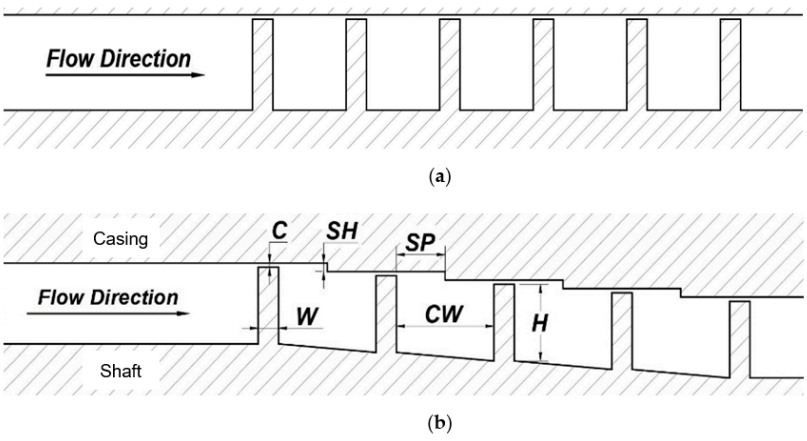

Figure 1. Labyrinth seal geometrical sketch and parameters. (**a**) Straight-through seal (**b**) Stepped seal.

So far, we developed a model or equation that can predict the flow of a straight labyrinth seal. In addition, a study was conducted to reduce the discharge coefficient by changing some shape parameters of the straight labyrinth seal [19,21,25,27,29]. Applying a straight labyrinth seal to the secondary flow path in which the shaft thickness changes is difficult. Therefore, a stepped labyrinth seal may be required. The stepped labyrinth seal has a shape with a step height (SH). Therefore, analyzing the discharge coefficient, including the shape variables that were previously considered for the straight labyrinth seal and the new shape variables of the stepped labyrinth seal, is necessary. Hence, in the present study, the pressure fields of the basic shape of straight and stepped labyrinth seals were compared and analyzed using RANS. The change in the discharge coefficient was investigated by adjusting the CW, SH, and step position (SP) of the stepped labyrinth seal, as shown in Figure 1.

When a numerical analysis was performed while each shape variable was varied, we classified it to have large and small discharge coefficients. According to previous studies [10,13,16,19,30], the cause of the change in the discharge coefficient was the change in the resistance due to pressure and that due to friction. Therefore, we selected and investigated the flow field, velocity field, and frictional wall resistance. Thus, the cause of the change in the discharge coefficient was investigated by comparing the flow patterns and wall shear stress of the large and small groups of a stepped labyrinth seal with the discharge coefficient.

2. Numerical Method and Verification

The index that is mainly used in labyrinth seals is the discharge coefficient, which is the actual mass-flow-rate ratio to the fluid that passes through the same cross-sectional area during the isentropic process. The isentropic equation is defined as shown below [16].

Isentropic mass flow rate:

$$\dot{m}_{id} = \frac{P_{in} A_c}{\sqrt{T_{in}}} \sqrt{\frac{2\gamma}{R(\gamma - 1)} \left[\left(\frac{P_{out}}{P_{in}} \right)^{\frac{2}{\gamma}} - \left(\frac{P_{out}}{P_{in}} \right)^{\frac{\gamma+1}{\gamma}} \right]} \tag{1}$$

Discharge coefficient:

$$C_d = \frac{\dot{m}}{\dot{m}_{id}} \tag{2}$$

To reduce the numerical analysis errors at the inlet and outlet and to observe the recirculation flow, the analysis was conducted by extending the distance by 64 and 50 mm at both ends of the tooth structure. Figure 2a shows the 17 million grid three-dimensional (3D) domain of the straight labyrinth seal; Figure 2b shows the grid near the tooth structure; and Figure 2c shows the grid of the stepped labyrinth seal. To sufficiently express the viscous sublayer, $y+ = 3$ or less needed to be satisfied.

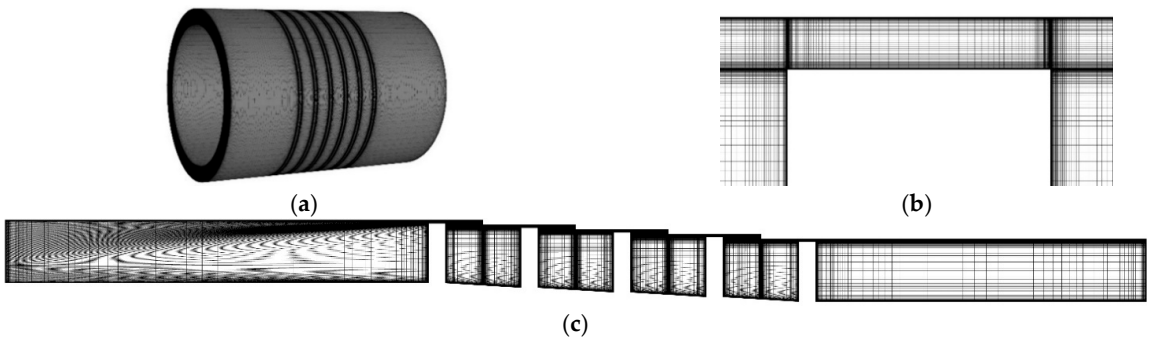

Figure 2. Computational domain of the straight-through seal. (**a**) Whole shape of the grids. (**b**) Enlarged part of the grids. (**c**) Computational domain of the stepped labyrinth seal.

Analyses were performed to confirm the sensitivity to the number of grids in two dimensions. From approximately 64,000 to 700,000 grids, alignment grids were created using ANSYS ICEM. In addition, ANSYS Fluent v20.1 was used as the solver. Figure 3 shows that 100,000 and 230,000 grids indicated a 0.1% difference in the discharge coefficient, and approximately 230,000 and 700,000 grids indicated a 0.2% difference. Although no feasibility problems occurred even when the analysis was performed on 100,000 grids, approximately 230,000 grids were used to sufficiently express the flow field.

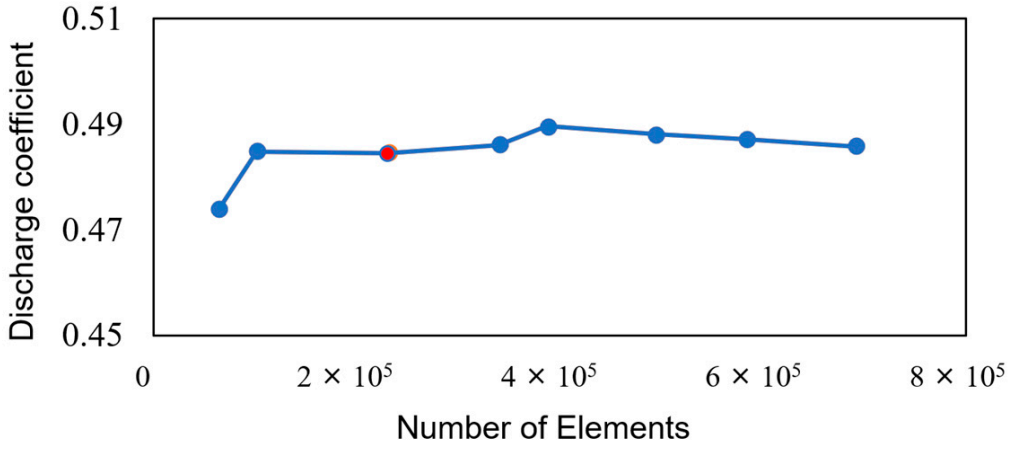

Figure 3. Grid test using the discharge coefficient.

Table 1 lists the length of each shape of the labyrinth seal. Because the labyrinth seal has a limited axial length, the straight labyrinth seal was adjusted to contain six teeth and the stepped labyrinth seal to have a five-tooth structure. The shape variables in this study were analyzed by selecting CW, SH, and SP. CW* and SH* were normalized to clearance, and SP* was normalized to the cavity width.

Table 1. Geometrical parameters of the labyrinth seals.

Geometry Parameter	Straight-Through Seal [16]	Stepped Seal
Number of teeth (N)	6	5
Clearance (C)	0.5 mm	0.5 mm
Tooth width (T)	2.5 mm	2.5 mm
Tooth height (H)	10.5 mm	10.5 mm
Cavity width (CW)	9.5 mm	3.5–33.5 mm
Step height (SH)	-	0–5.6 mm
Step position (SP)	-	0.15–10.35 mm

Table 2 lists the boundary conditions of the numerical analyses. The pressure and outlet were used, and the pressure ratio was 2.0. The numerical study was performed under adiabatic-wall conditions, with ideal gas at 300 K, and in stationary states.

Table 2. Boundary conditions of the numerical analyses.

Surface	Boundary Condition
Inlet	Pressure inlet, 300 K, 202,650 (Pa, absolute pressure)
Outlet	Pressure outlet, 300 K, 101,325 (Pa, absolute pressure)
Shaft	0 RPM, adiabatic wall
Casing	0 RPM, adiabatic wall

For the numerical analysis that used 2D axis symmetry, the 2D and 3D results were compared and analyzed, as shown in Figure 4. The difference was 0.03%, which verified the

validity of the 2D result. Figure 5 shows the sensitivity test of the turbulence model under the 2D-axis-symmetry conditions. As a reference value, the value tested by Wittig [16] was used. The SST *k*–ω model showed a maximum value of 8.4%, and the *k*–ε model showed the smallest gap of 0.7%. Therefore, all subsequent numerical analyses were carried out using the *k*–ε model.

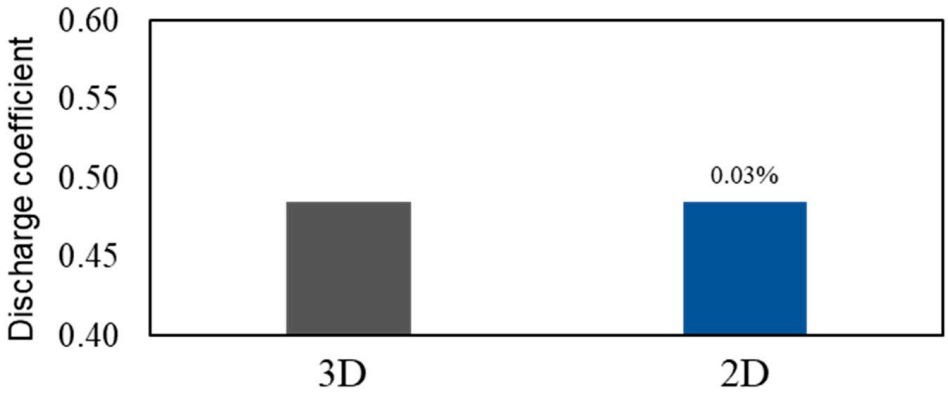

Figure 4. Comparison of the 2D and 3D discharge coefficients of the straight-through labyrinth seal.

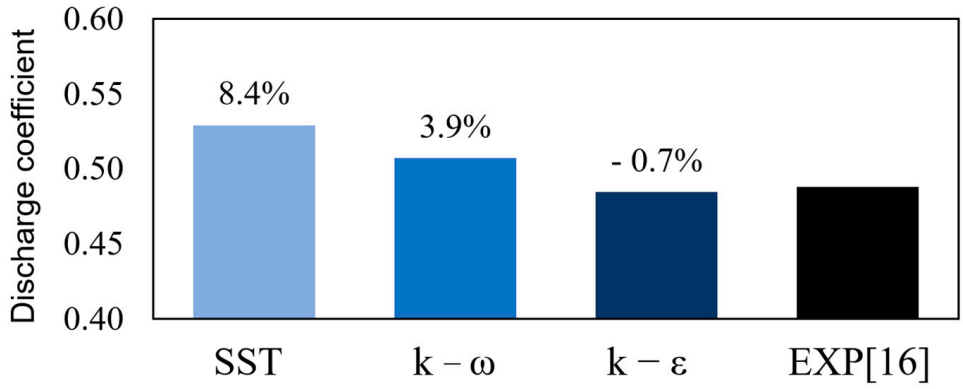

Figure 5. Prediction of the discharge coefficient using the turbulence model.

3. Results and Discussion

Figure 6 shows the discharge-coefficient values of each shape variable. The discharge coefficient was the most sensitive to the SH change. No significant changes were observed in CW*35, SH*1.4, or higher. When the SH change was small, the discharge coefficient was significantly larger than that of the straight labyrinth seal. When CW was changed, the discharge coefficient was the smallest in CW*7 and the largest in CW*67. Compared with CW*7, the discharge coefficient increased by 9.61% in CW*67. When the SH was changed, the discharge coefficient was the smallest in SH*1.6 and the largest in SH*0.2. Compared with SH*1.6, the discharge coefficient in SH*0.2 increased by 29.15%. When SP was changed, the discharge coefficient was the smallest in SP*0.7 and the largest in SP*0.2. Compared with SP*0.7, the discharge coefficient increased by 14.88% in SP*0.2.

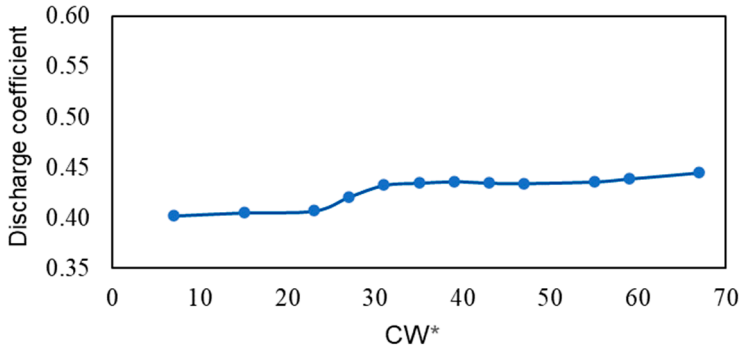

(**a**)

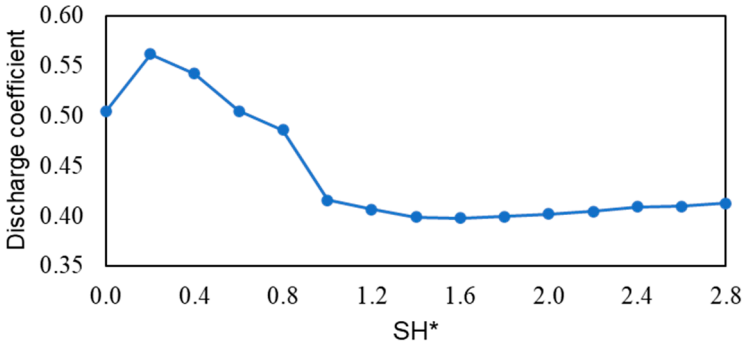

(**b**)

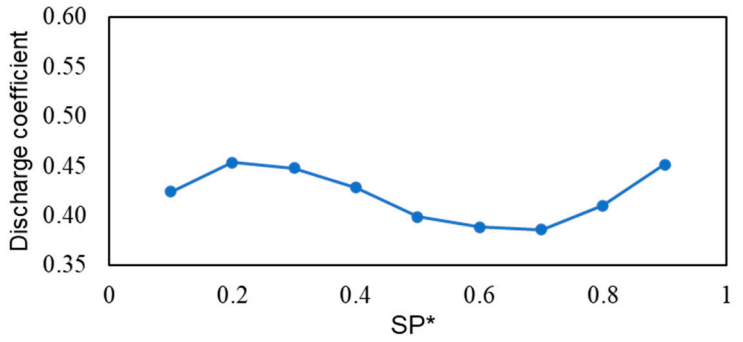

(**c**)

Figure 6. Prediction of the discharge coefficient according to the changes in the turbulence model discharge coefficient using geometrical parameters. (**a**) CW*. (**b**) SH*. (**c**) SP*.

Figure 7 shows that the straight labyrinth seal exhibited low pressure at the center of the cavity and high pressure at the clearance inlet. Meanwhile, in the stepped labyrinth seal, the pressure was down at the clearance inlet. Therefore, we could observe that the force that pushed the front was weak, and the leakage-flow rate was reduced. We examined the flow field for each shape to find out why the pressure was lowered at the inlet of the clearance inlet.

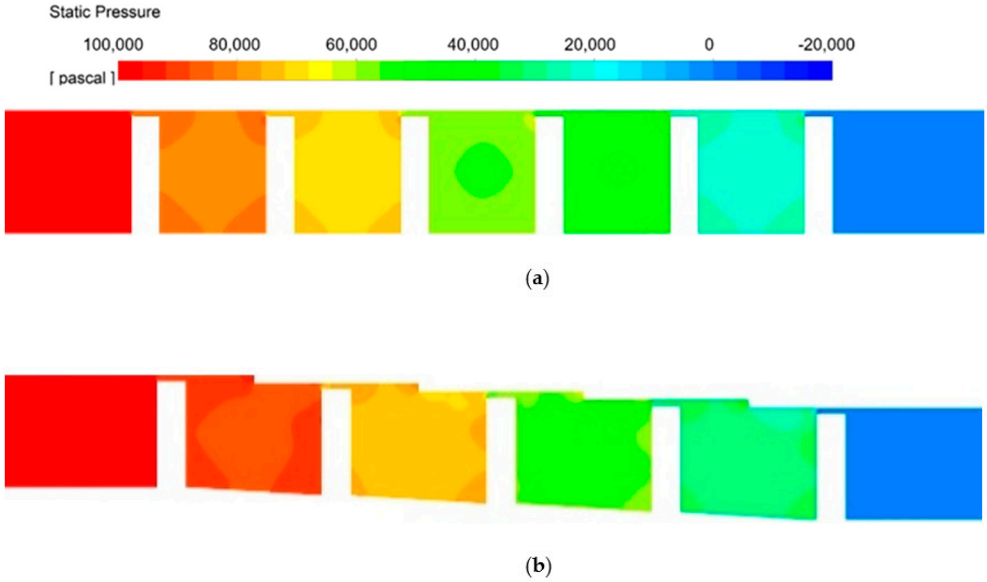

Figure 7. Contours of the labyrinth-seal static pressure. (**a**) Straight-through seal. (**b**) Stepped seal at SH*1.4.

Figure 8 compares the flow pattern according to the cavity width when the step was located at the center of the cavity. In Figure 8a, cases with large discharge coefficients are collected, and cases with small discharge coefficients are collected in Figure 8b. In the cases shown in Figure 8a, a primary bubble behind the tooth filled about half of the cavity, and a secondary bubble occurred with a similar size. On the other hand, in the geometries in Figure 8b, the primary bubble almost filled the entire cavity.

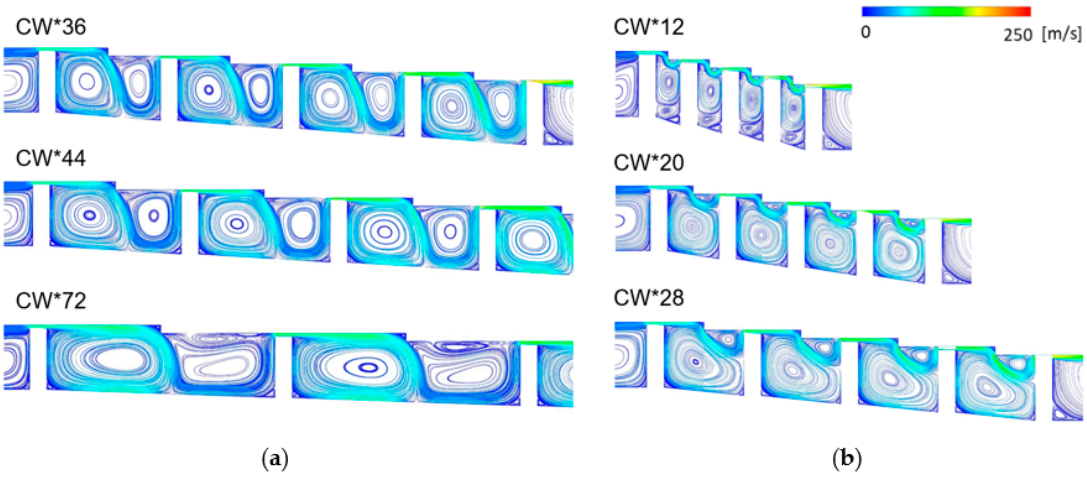

Figure 8. Change in the cavity flow structure according to CW*. (**a**) High-discharge-coefficient group. (**b**) Low-discharge-coefficient group.

Figure 9 illustrates the flow patterns according to the step height. The discharge coefficient significantly decreased in geometries where the step height was more than 1.4 times the clearance (Figure 9b). In the cases in Figure 9a, the flow pattern was similar to a straight-through seal, because the flow separation bubble did not occur greatly at the step. However, in the geometries in Figure 9b, a strong separation bubble was generated at the step position and continued to the end of the cavity.

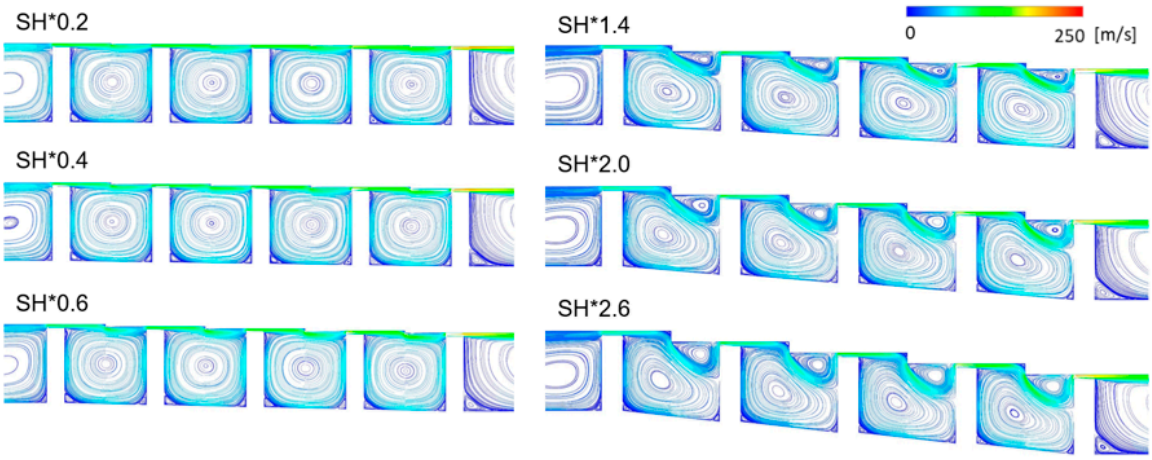

Figure 9. Change in the cavity flow structure according to SH. (**a**) High-discharge-coefficient group. (**b**) Low-discharge-coefficient group.

Figure 10 shows the flow changes that occurred depending on the relative position of the steps. If the step was located upstream (SP*02, SP*0.3 in Figure 10a), the separation bubble generated at the step was reattached in front of the tooth. When the step position moved beyond the middle of the cavity (Figure 10b), the separation bubble generated from the step continued to the next tooth, showing good sealing performance. However, if the step position was too close to the next tooth (SP*0.9 in Figure 10a), flow separation did not occur sufficiently at the step and did not contribute to sealing.

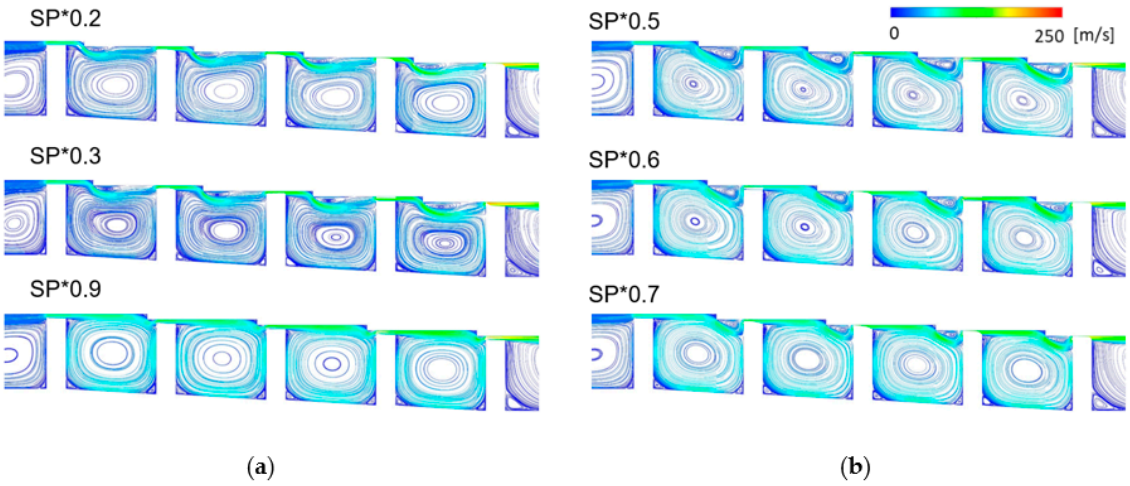

Figure 10. Change in the cavity flow structure according to SP. (**a**) High-discharge-coefficient group. (**b**) Low-discharge-coefficient group.

Figures 8–10 show that the shapes with small discharge coefficients experienced a small recirculation flow at the clearance inlet, which could be considered to obstruct the main flow. The recirculation flow that occurred at a source other than the gap inlet did not appear to be closely related to the discharge coefficient. In some shapes with a high discharge coefficient, the main flow was reattached to the downstream part of the recirculation flow and flowed into the clearance inlet.

Figure 11 shows that the vena-contracta size of the second to the fifth tooth structures in all shapes was very similar to that in the graph of the discharge coefficient. We could observe that the closer it was to T5, the larger was the vena contracta, which appeared to be caused by the high absolute speed.

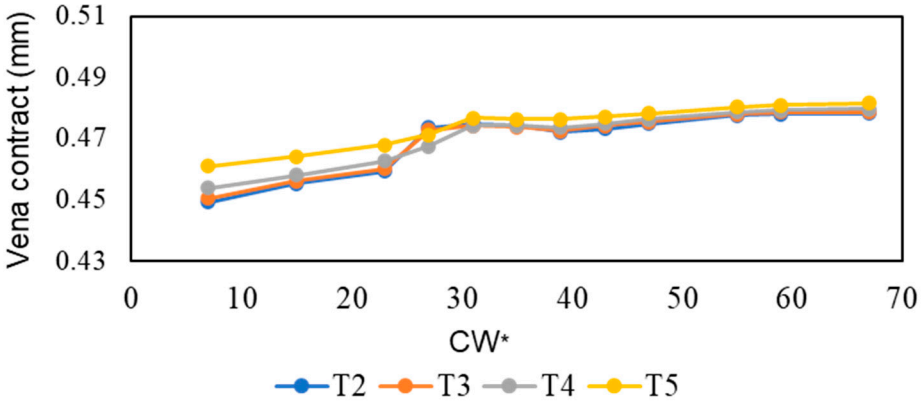

(**a**)

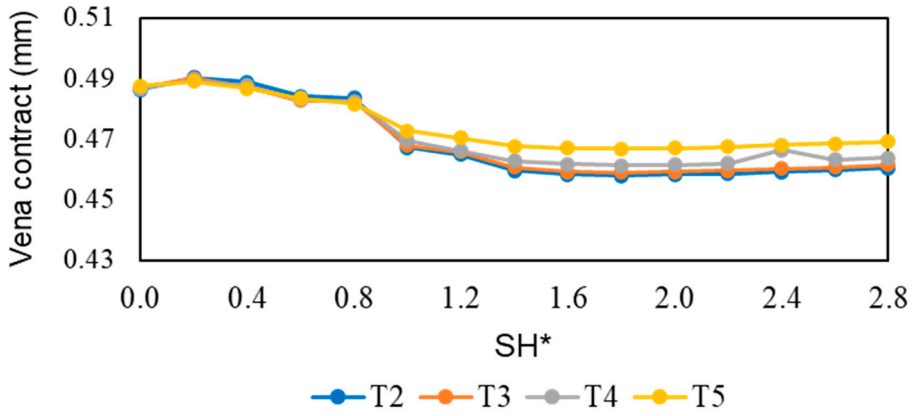

(**b**)

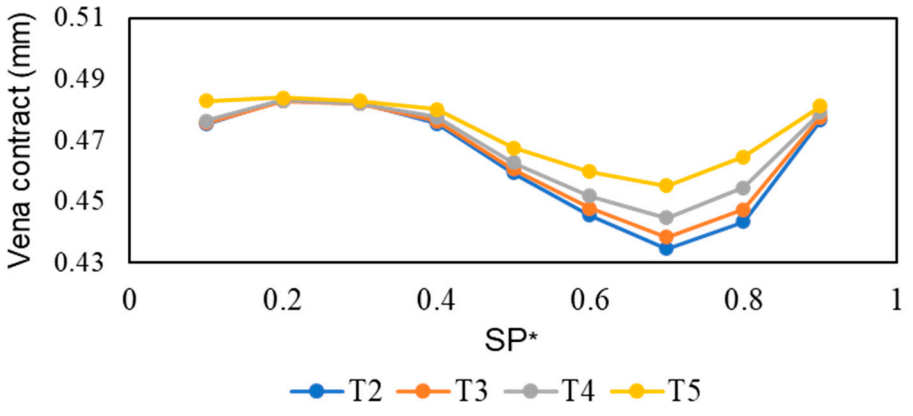

(**c**)

Figure 11. Vena-contracta changes due to geometrical parameters. (**a**) CW*. (**b**) SH*. (**c**) SP*.

Figure 12 shows the normalized axial velocity in the radial direction in the second-tooth structure and Cn. The solid lines indicate the shapes with large discharge coefficients, and the dotted lines indicate those with small discharge coefficients. The shapes with large discharge coefficients exhibited a steep increase in the axial speed at the clearance inlet, and those with small discharge coefficients exhibited a relatively gentle axial speed.

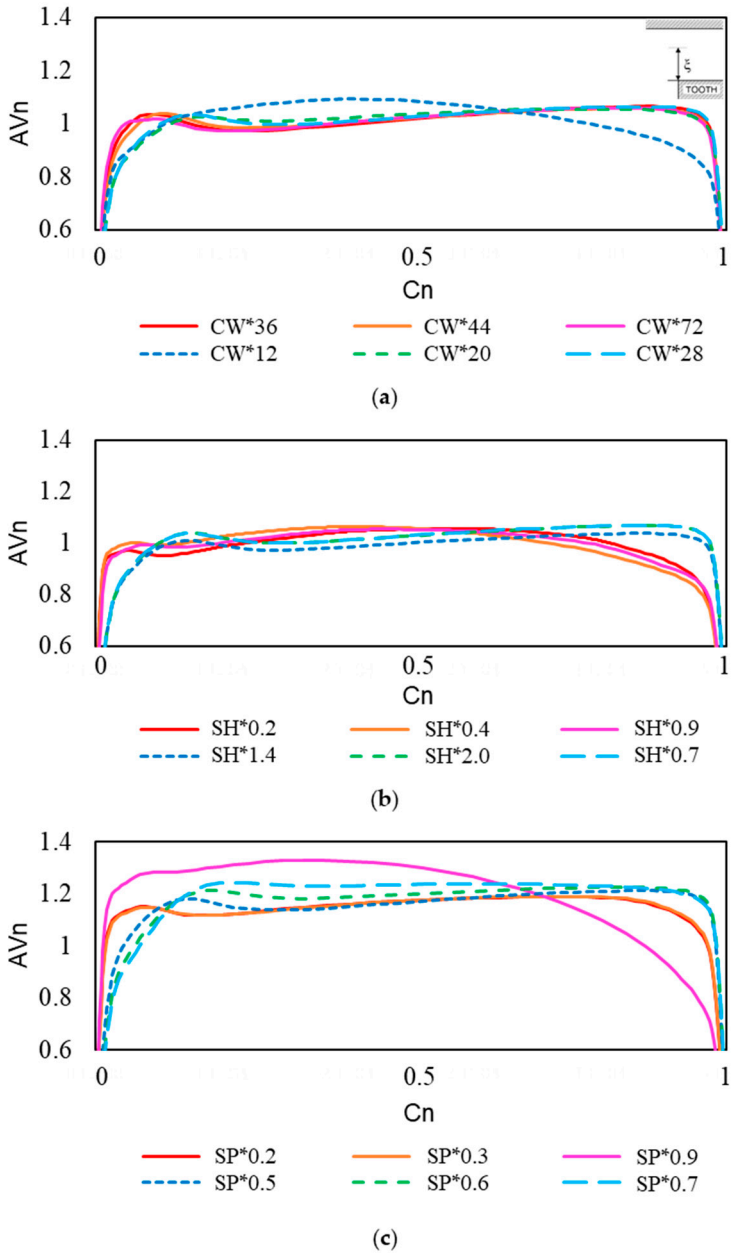

Figure 12. Normalized axial-velocity changes by geometrical parameter at the second tooth. (**a**) CW. (**b**) SH. (**c**) SP.

In Figure 12b, the steep difference in the radial and axial velocity of the group with the large discharge coefficient and the group with the small discharge coefficient was more pronounced than that of CW and SP. This is because the maximum value of the SH discharge coefficient was the largest compared with the minimum value. In Figure 12a, the difference in the steepness of the radial and axial velocities between the group with a large discharge coefficient and the group with a small discharge coefficient was insignificant compared with those of SH and SP. This is because the maximum value of the discharge coefficient of CW was the smallest compared with the minimum value.

Figure 13 shows the wall shear stress for each variable shape. For SH*, the wall shear stress was similar to the discharge coefficient, but not for CW* and SP*. Therefore, we could observe that the stepped labyrinth seal exerted a more negligible effect on the wall friction.

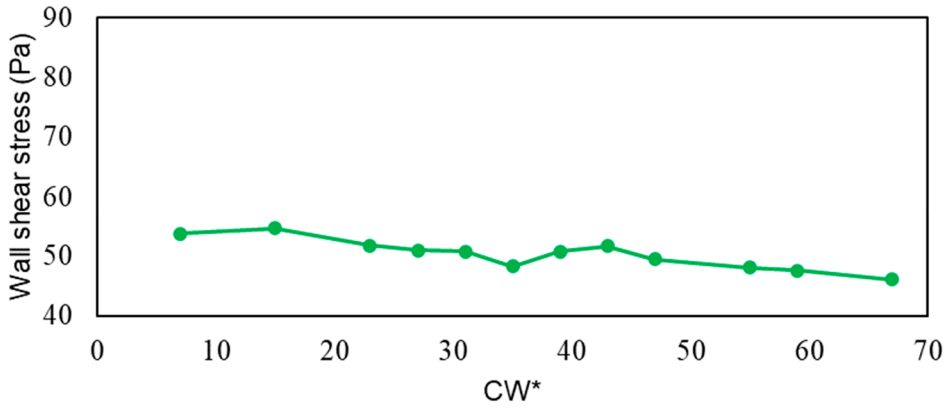

(**a**)

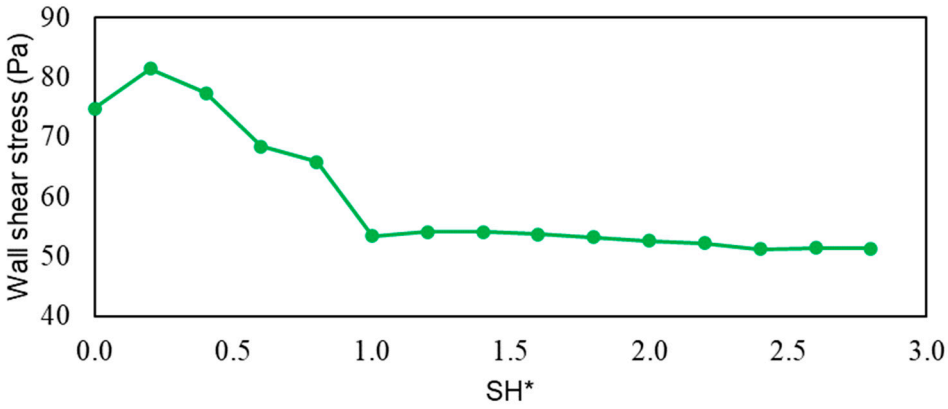

(**b**)

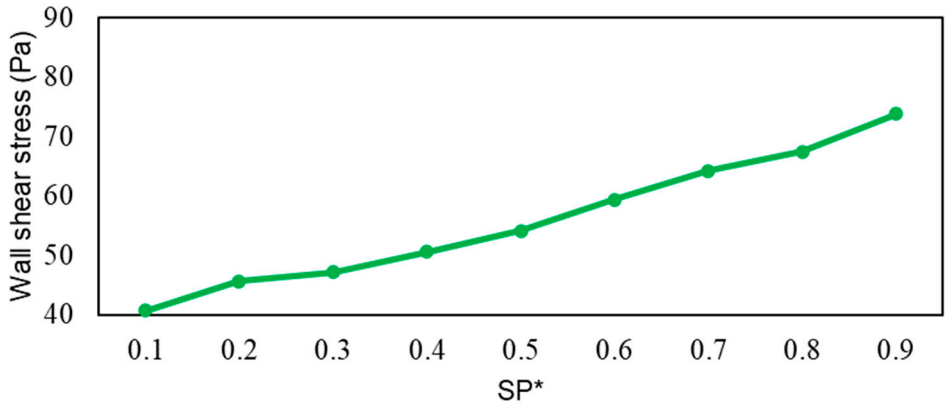

(**c**)

Figure 13. Changes in the wall shear stress of the geometrical parameters. (**a**) CW*. (**b**) SH*. (**c**) SP*.

4. Conclusions

Numerical analyses were performed by changing the different shape parameters of a stepped labyrinth seal, which is an advanced form of labyrinth seal widely used for sealing clearances. By observing the change in the discharge coefficient according to the change in each variable shape, the effect of reducing the discharge coefficient of the stepped labyrinth

seal compared with that of the straight labyrinth seal under the condition of the same axial length was quantitatively evaluated.

1. In the stepped labyrinth seal, when CW, SH, and SP were varied, the discharge coefficient of SH was the most sensitive at a factor of approximately 30%;
2. In the stepped labyrinth seal, when a small recirculation flow appeared at the clearance inlet, the clearance inlet pressure was reduced, and the axial velocity gently increased, which reduced the size of the vena contracta. The shapes with these characteristics exhibited a small discharge coefficient;
3. The wall shear stress and discharge coefficient trends were very similar for the SH changes of the stepped labyrinth seal. However, no correlations existed between the wall shear stress and the discharge coefficient for CW and SP changes.

Author Contributions: Y.H.C. carried out the simulations, analyzed the CFD data, and wrote the paper. J.A. supervised the research, analyzed the CFD data, and wrote the paper. All authors have read and agreed to the published version of the manuscript.

Funding: This work was supported by the Agency for Defense Development Grant funded by the Korean Government (UD220004JD).

Institutional Review Board Statement: Not applicable.

Informed Consent Statement: No applicable.

Data Availability Statement: Data are contained within this article.

Conflicts of Interest: The authors declare no conflict of interest.

Nomenclature

A_c	Cross-sectional area of labyrinth seal (m^2)
AVn	Normalized axial velocity $\text{AVN} = \frac{\text{local axial velocity}}{\text{average axial velocity}}$
C_d	Discharge coefficient
C_n	Normalized clearance $C_n = \frac{\xi}{\text{clearance}}$
CW	Cavity width
$\dot{m}$	Mass flow rate (kg/s)
P	Pressure (Pa)
R	Specific gas constant
SH	Step height
SP	Step position
T	Temperature (K)
W	Width of tooth
Greek Symbols	
γ	Isentropic coefficient
ξ	Coordinate from tooth tip
Subscripts	
id	Ideal
in	Inlet
out	Outlet
Superscript	
*	Normalized

References

1. Boyce, M.P. *Gas Turbine Engineering Handbook*; Elsevier: Amsterdam, The Netherlands, 2011.
2. Ahn, J.; Song, J.C.; Lee, J.S. Fully Coupled Large Eddy Simulation of Conjugate Heat Transfer in a Ribbed Channel with a 0.1 Blockage Ratio. *Energies* **2021**, *14*, 2096. [CrossRef]
3. Goldstein, R.J.; Eckert, E.R.G.; Ramsey, J.W. Film Cooling with Injection Through Holes: Adiabatic Wall Temperatures Down-394 Stream of a Circular Hole. *J. Eng. Power* **1968**, *90*, 384–393. [CrossRef]

4. Zhou, B. PowerGen Gas Turbine Losses and Condition Monitoring: A Loss Data-Based Study. *ASCE-ASME J. Risk Uncertain. Eng. Syst. B: Mech. Eng.* **2016**, *2*, 021007. [CrossRef]
5. Sultanian, B.K. *Gas Turbines Internal Flow Systems Modeling*; Cambridge University Press: Cambridge, UK, 2018.
6. Martin, H.M. Labyrinth Packings. *Engineer* **1908**, *85*, 35–36.
7. Zhang, W.; Zhang, Y.; Yang, J.; Li, C. Influence of Tilting Rotor on Characteristics of Fluid-Induced Vibration for Labyrinth Seals. *J. Vibroeng* **2016**, *18*, 5416–5431. [CrossRef]
8. Holle, G.; Krishnan, M. Gas Turbine Engine Brush Seal Applications. In Proceedings of the 26th Joint Propulsion Conference, Orlando, FL, USA, 18 July 1990.
9. Bondarenko, G.A.; Khizhnyak, L.A. Experimental Investigation of a Honeycomb Seal. *Chem. Petrol. Eng.* **1978**, *14*, 793–795. [CrossRef]
10. Becker, E. Strömungsvorgänge in Ringformigen Spalten (Labyrinth-Dichtungen). *Ver. Deut Ing.* **1907**, *51*, 1133–1141.
11. Stodola, A. *Steam and Gas Turbines*, 6th ed.; McGraw-Hill: New York, NY, USA, 1927; pp. 189–194.
12. Egli, A. The Leakage of Steam Through Labyrinth Seals. *Trans. ASME* **1935**, *57*, 115–122.
13. Dollin, F.; Brown, W.S. Flow of Fluids Through Openings in Series. *Engineer* **1937**, *164*, 223–224.
14. Hodkinson, B. Estimation of the Leakage Through a Labyrinth Gland. *Proc. Inst. Mech. Eng.* **1939**, *141*, 283–288. [CrossRef]
15. Jeri, J. Flow Through Straight-Through Labyrinth Seals. In Proceedings of the Seventh International Congress on Applied Mechanics, London, UK, 5–11 September 1948; 1948; Volume 2, pp. 70–82.
16. Wittig, S.; Schelling, U.; Kim, S.; Jacobsen, K. Numerical Predictions and Measurements of Discharge Coefficients in Labyrinth Seals. In Proceedings of the ASME 1987 International Gas Turbine Conference and Exhibition, Anaheim, CA, USA, 31 May–4 June 1987.
17. Denecke, J.; Dullenkopf, K.; Wittig, S.; Bauer, H.-J. Experimental Investigation of the Total Temperature Increase and Swirl Development in Rotating Labyrinth Seals. *ASME J. Turbomach.* **2005**, *3*, 1161–1171.
18. Szymanski, A.; Dykas, S.; Wroblewski, W.; Fraczek, D. Experimental and Numerical Validation Study of the Labyrinth Seal Configurations. In Proceedings of the 12th European Conference on Turbomachinery Fluid Dynamics & Thermodynamics ETC12, Stockholm, Sweden, 3–7 April 2017.
19. Baek, S.I.; Ahn, J. Optimizing the Geometric Parameters of a Straight-Through Labyrinth Seal to Minimize the Leakage Flow Rate and the Discharge Coefficient. *Energies* **2021**, *14*, 705. [CrossRef]
20. Eser, D.; Kazakia, J.Y. Air Flow in Cavities of Labyrinth Seals. *Int. J. Eng. Sci.* **1995**, *33*, 2309–2326. [CrossRef]
21. Wein, L.; Kluge, T.; Seume, J.R.; Hain, R.; Fuchs, T.; Kähler, C.; Schmierer, R.; Herbst, F. Validation of RANS Turbulence Models for Labyrinth Seal Flows by Means of Particle Image Velocimetry. In *Proceedings of the ASME Turbo/Expo, Virtual, Online, 21–25 September 2020*; ASME: New York, NY, USA, 2020; Volume 10A.
22. Gao, F.; Chew, J.W.; Beard, P.F.; Amirante, D.; Hills, N.J. Numerical Studies of Turbine Rim Sealing Flows on a Chute Seal Configuration. In Proceedings of the ETC 12, Stockholm, Sweden, 3–7 April 2017; Rolls-Royce Plc: Derby, UK, 2017.
23. Stocker, H.L. Determining and Improving Labyrinth Seal Performance in Current and Advanced High Performance Gas Turbines. *AGARD Conf. Proc.* **1978**, *237*, 13/1–13/22.
24. Wittig, S.; Jacobsen, K.; Schelling, U.; Kim, S. Heat Transfer in Stepped Labyrinth Seals. *J. Eng. Gas Turbines Power* **1988**, *110*, 63–69. [CrossRef]
25. Vakili, A.D.; Meganathan, A.J.; Michaud, M.; Radhakrishnan, S. An Experimental and Numerical Study of Labyrinth Seal Flow. In Proceedings of the Turbo Expo, Reno, NV, USA, 6–9 June 2005; pp. 1121–1128.
26. Joachimmiak, D.; Krzyślak, P. Analysis of the Gas Flow in a Labyrinth Seal of Variable Pitch. *J. Appl. Fluid Mech.* **2019**, *12*, 921–930. [CrossRef]
27. Hur, M.S.; Lee, S.I.; Moon, S.W.; Kim, T.S.; Kwak, J.S.; Kim, D.H.; Jung, I.Y. Effect of Clearance and Cavity Geometries on Leakage Performance of a Stepped Labyrinth Seal. *Processes* **2020**, *8*, 1496. [CrossRef]
28. Zhao, Y.; Wang, C. Shape Optimization of Labyrinth Seals to Improve Sealing Performance. *Aerospace* **2021**, *8*, 92. [CrossRef]
29. Kim, J.H.; Ahn, J. Large Eddy Simulation of Leakage Flow in a Stepped Labyrinth Seal. *Processes* **2021**, *9*, 2179. [CrossRef]
30. Deng, S.; Wang, D.; Chen, X. Experimental Investigation of Geometry Effect on Discharge Characteristic for Stepped Labyrinth Seal. In Proceedings of the Montreal 2018 Global Power and Propulsion Forum, Montreal, QC, Canada, 7–9 May 2018.